Separation Science and Technology
Publication details, including instructions for authors and subscription information:
http://www.informaworld.com/smpp/title~content=t713708471

Hydraulic Testing of Ion Exchange Resins for Cesium Removal from Hanford Tank Waste

K. P. Brooks[a]; B. S. Augspurger[a]; D. L. Blanchard[a]; J. M. Cuta[a]; S. K. Fiskum[a]; M. R. Thorson[b]
[a] Pacific Northwest Division, Battelle, Richland, Washington, USA [b] Bechtel National Incorporated, Richland, Washington, USA

To cite this Article Brooks, K. P. , Augspurger, B. S. , Blanchard, D. L. , Cuta, J. M. , Fiskum, S. K. and Thorson, M. R.(2006) 'Hydraulic Testing of Ion Exchange Resins for Cesium Removal from Hanford Tank Waste', Separation Science and Technology, 41: 11, 2391 — 2408
To link to this Article: DOI: 10.1080/01496390600742724
URL: http://dx.doi.org/10.1080/01496390600742724

Separation Science and Technology, 41: 2391–2408, 2006

ISSN 0149-6395 print/1520-5754 online
DOI: 10.1080/01496390600742724

Hydraulic Testing of Ion Exchange Resins for Cesium Removal from Hanford Tank Waste

K. P. Brooks, B. S. Augspurger, D. L. Blanchard, J. M. Cuta, and S. K. Fiskum
Battelle, Pacific Northwest Division, Richland, Washington, USA

M. R. Thorson
Bechtel National Incorporated, Richland, Washington, USA

Abstract: The granular ion exchange resin SuperLig® 644 is the ion exchange resin of choice for ^{137}Cs separation from Hanford tank wastes. Current testing activities are evaluating both ground gel and spherical resorcinol-formaldehyde (RF) resins as alternatives to the sole-source supplied SL-644 while achieving comparable loading and elution performance. The purpose of this testing was then to compare the bed forces, resin particle breakage, and differential pressure across the resin bed during multiple load-elute cycles. These tests were conducted in a small-scale column with high flow rates to simulate the hydraulic conditions that would be experienced in a full-scale column.

Keywords: Organic ion exchange resins, hydraulic tests, permeability, compressibility

INTRODUCTION

The U.S. Department of Energy (DOE) is responsible for the disposition of millions of gallons of high-level radioactive waste slurries stored at the Hanford site in Washington State. The waste is to be vitrified following specific pretreatment processing, separating the waste into a relatively

Received 11 January 2006, Accepted 20 March 2006
Address correspondence to K. P. Brooks, Battelle, Pacific Northwest Division, Mail Stop K6-24, P.O. Box 999, Richland, Washington 99352, USA. Tel.: (509) 376-2233; Fax: (509) 376-3108; E-mail: kriston.brooks@pnl.gov

small-volume high-activity waste fraction and a large-volume low-activity waste (LAW) fraction in the River Protection Project-Waste Treatment Plant (RPP-WTP). Cesium-137 will be separated from the liquid portion of the waste slurry (supernate) to facilitate easier maintenance of the LAW vitrification equipment and near-surface disposal at Hanford of the vitrified LAW. The current pretreatment flowsheet includes the use of a cesium-selective, elutable, organic ion exchange material, SuperLig® 644 (SL-644) for this separation. This material has been developed and supplied by IBC Advanced Technologies, Inc in American Fork, UT. To provide an alternative to this sole-source resin supply, work is being performed to select an alternative ion exchange resin for Cs removal. Resorcinol-formaldehyde (RF) resin was selected as the most viable alternative (1). Two different forms of these resins were developed for alternative testing: ground gel resin similar in physical form to the SL-644 and a spherical RF resin.

Both the SL-644 and RF resins expand in the sodium form appropriate for cesium separation and contract in the acid form during elution. SL-644 expands by up to 50% in sodium form. This results in significant differences in resin bed height within the ion exchange column. Previous testing with SL-644 has shown that high column fluid pressure drops and wall pressures were experienced during the loading step after multiple operating cycles (2). Several reasons for the observed elevated pressures were originally considered, including

1. fines that plug the column generated from osmotic shock resulting from cycling the resin between acid and sodium form,
2. high particle breakage and fines generation from wall and internal friction upon resin expansion during regeneration,
3. bed compaction from compressive force due to flow-pressure drop, resulting in even higher pressure drops.

Although fines generation from osmotic shock can be performed simply by cycling the resin between acid and sodium forms, the other two possible reasons for fines generation and elevated column pressures are difficult to perform on a small scale. Large scale tests require not only expensive columns and resin volumes, but the extremely large volumes of feed, eluant, and regenerate feedstock needed for multiple cycle tests are expensive to produce and disposition. There is a need to find methods to perform simple tests that can produce similar internal friction upon resin expansion and contraction and similar bed compaction due to flow pressure drop.

Battelle, Pacific Northwest Division, and Bechtel National Incorporated has developed an approach to simulate the hydraulic conditions that would be experienced in a full-scale column using high flow rates in a geometrically similar bench-scale column. This was done by increasing the superficial velocity in the column by the ratio of the full-scale and bench-scale column heights. By doing so, the testing time and expense can be reduced and the hydraulic characteristics of ion exchange resins such as RF and SL-644 can be compared.

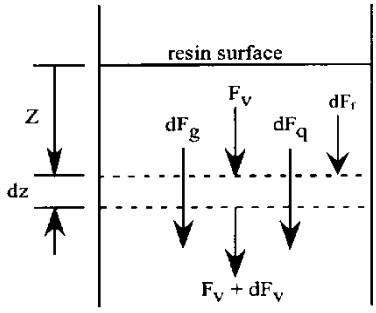

Figure 1. Axial force balance on differential section of contracting resin bed.

THEORY

The resin bed in the ion exchange column is treated as a one-dimensional system, as illustrated in Fig. 1. The differential axial stress in the bed can be expressed in terms of the force balance on a differential 'slice' of the bed,

$$dF_v = A_{IX} dP_s = dF_g + dF_q - dF_f \tag{1}$$

where dF_g = buoyancy force $= (\rho_s - \rho_l)(1 - \varepsilon_p)(1 - \varepsilon) g A_{IX} dz$

$$dF_q = \text{hydraulic drag force} = \frac{C_D \mu V_0 (1 - \varepsilon)^2}{\Phi_s^2 D_p^2 \varepsilon^3} A_{IX} dz$$

$$dF_f = \text{friction drag force} = -\frac{4\mu' k'}{D} A_{IX} dz$$

This yields an expression for the axial stress, in the form

$$\frac{dP_s}{dz} = (\rho_s - \rho_l)(1 - \varepsilon_p)(1 - \varepsilon) g + \frac{C_D \mu V_0}{\Phi_s^2 D_p^2} \frac{(1 - \varepsilon)^2}{\varepsilon^3} + 4 \frac{\mu' k'}{D} P_s \tag{2}$$

where

A_{IX} = cross-sectional area of column

P_s = bed axial stress

D_p = particle diameter

D = column diameter

V_0 = superficial velocity of the fluid

g = gravitational acceleration

k' = radial to axial stress ratio

ε_p = pore density

ε = bed porosity

μ = liquid viscosity

μ' = coefficient of friction

ρ_s = solid density

ρ_l = liquid density

Φ_s^2 = particle sphericity

C_D = form drag coefficient

This is a typical formulation for representing flow in a packed bed (3). The first term on the left-hand side represents the buoyancy force on the particles in the bed, the second term represents the effect of form drag due to the fluid flowing over the particles in the bed for laminar flow, and the third term represents the friction forces in the bed due to movement of the particles as the particles slide along the wall or against adjacent particles during expansion or contraction of the bed. When the particles are expanding, the net movement is in the upward direction, and the sign of the friction term is positive, as shown in Eq. (2). In the expansion phase, the friction forces act in the same direction as the fluid drag, and tend to increase the axial stress. In the contraction phase, the friction forces act in the opposite direction from the fluid drag, and tend to relieve axial stresses.

During the expansion phase, the axial and radial stresses increase until they are sufficient to induce particles to slide upward along the walls of the column and against each other. If the friction forces are strong enough to prevent movement of the particles within the bed, radial stresses will grow until they exceed either the yield stress of the bed material or that of the structure containing the bed. In the first case, the bed material will undergo undesirable fracturing and fragmentation; in the other, the column will swell and possibly burst.

In small scale testing to determine the effect of stresses due to expansion of the bed, it is important to produce forces in the test section that are comparable to the forces expected in the full-scale ion exchange column. If the test column has the same length-to-diameter ratio as the full-scale column, the friction force term will be the same in the test column as in the full-scale column, when integrated over the height of the column. But because the measurement of interest is the total axial and radial stress in the full-scale ion exchange column, appropriate testing in columns of smaller diameter requires sacrificing some aspects of dimensional similitude in the test conditions. The buoyancy force term will be smaller in the test column than in the full scale column. If the flow velocity in the test column is the same

magnitude as the velocity in the full scale column, the fluid drag term will also be smaller than in the full scale column. In that case, the total axial and radial stress in the test column will be significantly less than what would be obtained in the full scale column at the same flow rate.

The fluid drag term is the only one of the three components of Eq. (2) that can be adjusted in the testing processes to achieve forces in the small scale test column that will produce axial and radial stresses of the same magnitude as in the full scale column. By increasing the flow velocity in the bed (V_0) while decreasing the bed height (L) by the same ratio, the fluid drag forces for a small column will give fluid drag forces equivalent to those seen in the full scale column as long as the flow within the bed is laminar. This relationship can be shown as,

$$(V_0)_{sc} = (V_0)_{IXcol.}\left(\frac{L_{IX}}{L_{sc}}\right) \tag{3}$$

where

L_{IX} = bed height in full scale IX column

L_{sc} = bed height in small column

$(V_0)_{\mathrm{IXcol}}$ = flow velocity in full scale IX column

$(V_0)_{sc}$ = flow velocity in small column

In this case the pressure drop across the small scale column is equal to that seen in the full scale column. The one limitation of this approach is that the buoyancy force on the bed will be too small by a factor of L_{IX}/L_{ts}. There is no simple adjustment that can be made in the test design that can compensate for this. However, the difference in density between the ion exchange resins and the solutions tested is very small ($\sim$0.1 g/cc). Another limitation is that in small column, high flow rates results in the entire bed expanding simultaneously. In contrast, in a large column, the resin would expand from the top. This may allow the bed to expand more slowly and produced smaller internal forces. In any case, this approach allows a reasonable comparison between materials tested under similar hydraulic conditions.

EXPERIMENTAL

The SL-644 granular resin, RF granular resin, and the spherical RF resin were pretreated by cycling twice from the H-form to Na-form in a beaker. Each resin was converted to the H-form by contacting it with 0.5 M HNO_3 for 1 hour. The acid was then decanted, and the resin was rinsed with deionized (DI) water until the solution pH was $>$5. The resin was then contacted with 0.25 M NaOH for 1 hour and then rinsed with DI water

until the solution pH was <10. Following pretreatment, the wet sodium form ion exchange resins were loaded into 5 cm diameter, 20-cm-long glass columns. Glass pressure ports were installed on the top and bottom of the column to measure the differential pressure across the resin bed using differential pressure transducers. Each resin was tested at two height to diameter ratios. The volume of ion exchange resin tested in the sodium form and for the respective H/D ratios are shown in Table 1. The resins were tested in the order presented in the table. These height to diameter ratios are larger than planned for the full-scale column. However, they were used to assure that measurable internal pressures and particle breakage could be observed.

A complete cycle includes six steps:

1. loading with a simulated tank waste,
2. waste displacement,
3. water rinse,
4. acid elution,
5. water rinse, and
6. regeneration.

The flows and concentrations for each of these steps are provided in Table 2. The supernate waste stored in the Hanford tank designated 241-AP-101 (AP-101) was simulated according to a recipe developed previously (4). This simulated AP-101 waste was then prepared by Noah Technologies (San Antonio, TX) at 5 M sodium concentration with all of the major inorganic ions found in the actual waste. Non-radioactive cesium ion was used at a concentration of 6 μg/mL. The simulated AP-101 waste had a density of 1.23 g/mL and a viscosity of 2.6 cp at 24°C.

Since these organic ion exchange resins may expand during loading and do expand during regeneration, the accelerated flow experiments were performed during these steps when high resin pressures are expected. During the water rinse steps and acid elutions, the resins are either contracting

Table 1. Resins evaluated during for permeability testing[a]

	Actual resin height to diameter ratio		Actual resin volume (mL)	
Characteristics	Column A	Column B	Column A	Column B
SL-644	1.88	2.72	184	267
RF Spherical	1.56	2.8	153	274
RF Granular	1.52	2.78	149	273

[a]Height and volume measured after first displacement step.

Table 2. Processing steps for the permeability testing

Process step	Flowrate (s)	Volume or time	Measurements
Cycle 1			
Load: AP-101 Simulant	1600, 1200, 800 mL/min	30, 30, 30 min (re-circulated flow)	Flowrate Pressure drop Load cell force Resin height Temperature Viscosity/density
Displacement: 0.1 M NaOH	3 BV/h	3 BV	Resin height
Rinse: DI Water	3 BV/h	3 BV	Resin height
Elute: 0.5 M HNO3	6 BV/h	12 BV	Resin height
Rinse: DI Water	1.4 BV/h	3 BV	Resin height
Regenerate: 1 M NaOH	1600, 1200, 800 mL/min	90, 30, 30 min (re-circulated flow)	Flowrate Pressure drop Load cell force Resin height Temperature Viscosity/density
Cycle 2			
Same as Cycle 1, except only measure permeability at 1600 mL/min flowrate			
Cycle 3			
Same as Cycle 1, except only measure permeability at 1600 mL/min flowrate			
Cycle 4			
Same as Cycle 1			

or stationary. Thus, these steps were peformed at much lower flowrates, consistent with the number of bed volumes per hour expected during full-scale plant operations.

The full scale column design that was the basis for these experiments has a diameter of 48″ and a resin height of 54″. At a flow of 15 gpm of Hanford tank waste supernatant, the columns were expected to have a pressure drop of 4 psi. To match the forces expected in the full-scale column, the superficial velocity of 4.8 cm/min was increased to 81 cm/min in the small-scale column (a flow of 1550 mL/min). The conditions tested were selected to bound the nominal flow rate. To minimize the amount of chemicals required, the reagents were recycled during the high-flow tests. A sufficient quantity of caustic is maintained in the loop to prevent large swings in solution chemistry during the run.

During each loading and regeneration step, the flowrate, pressure drop, resin bed height, and temperature are measured every 10 minutes during the recirculation time. At the end of the run, samples were pulled for viscosity

and density measurements. These measurements were used to determine the permeability of the ion exchange bed during the run.

The resin bed was held in place on a porous polypropylene cylindrical plug (See Fig. 2). This plug raised the resin up to the height of the bottom pressure port and housed the bottom load cell. A 0.25-in.-diameter pin was flush-mounted with the resin bed. When force was exerted downward, the pin transferred the force to a miniature load cell within the plug. A similar arrangement was also provided on the side of the column to measure radial forces at the bottom of the column. The resin was prevented from passing through the porous plug by a plastic screen.

Following the permeability tests, a compressibility test was performed by applying a known force on the top of a resin bed and measuring the change in bed height. A schematic of the test apparatus is shown in Fig. 3. The test was performed by using the same 5-cm-diameter columns and apparatus as were used in the permeability studies. In addition, an elastic membrane above the bed was pressurized with water to produce force on the top of the resin bed. The resin itself was in simulated AP-101 supernate. The plastic pressure disk at the bottom assured that the membrane applied an even distribution of pressure across the resin surface, and the pressure disk at the top prevented the water used to pressurize the membrane from mixing with the simulated AP-101 supernate in the resin bed. The bottom of the column allowed the simulated supernate to flow out as the resin bed compressed.

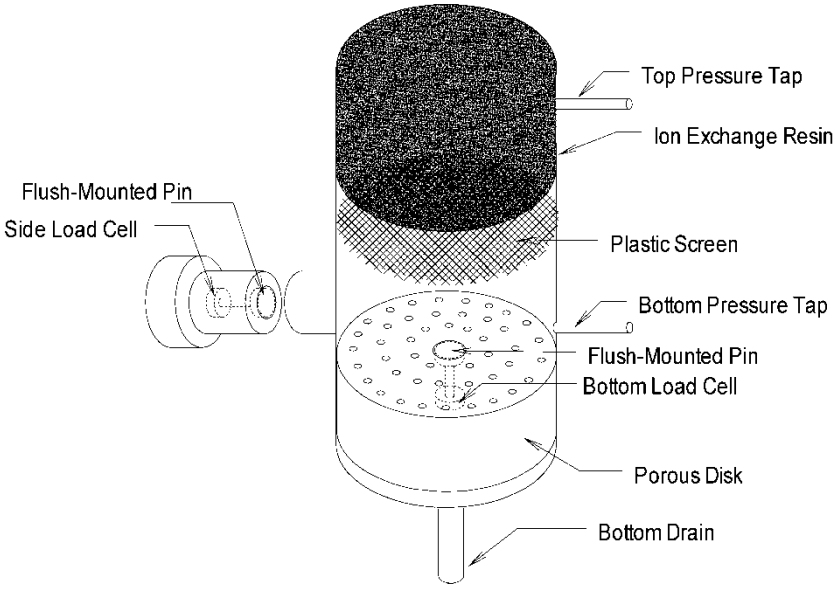

Figure 2. Schematic of the ion exchange column load cell and differential pressure sensor placement in the bench-scale hydraulic testing system.

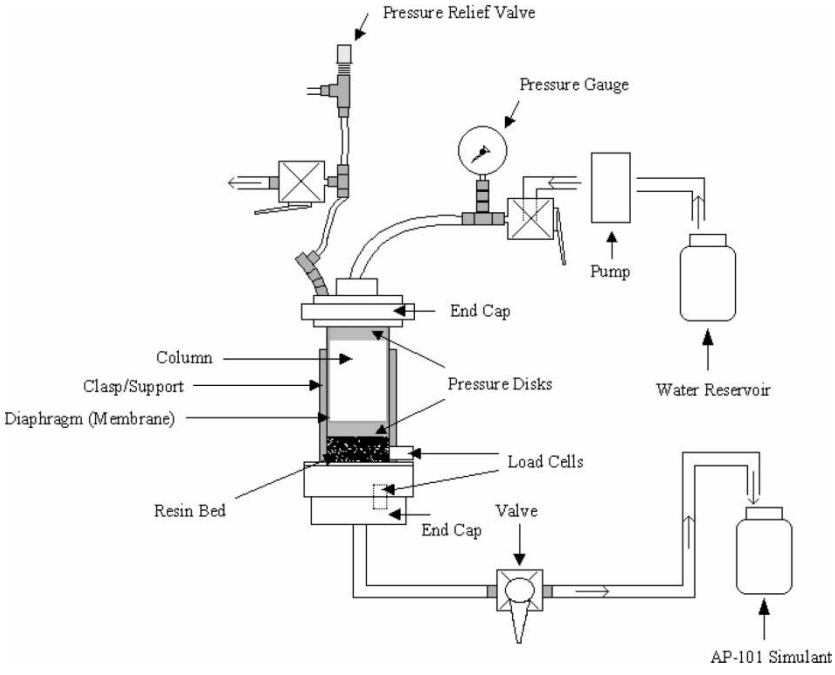

Figure 3. Schematic of the compressibility test equipment.

The pressure on the bed was increased stepwise to 20 psi by turning on and off the positive-displacement feed pump. The pressure was decreased stepwise by opening a valve at the top of the column and allowing the simulated supernate forced out during the compression to flow back into the column.

RESULTS

The pressure drop across the columns during a complete cycle for a representative ion exchange resin is shown in Fig. 4 and compared to the expected pressure drop for the full-scale column. As can be seen from the figure, the pressure drops experienced within the small-scale column do bound the conditions expected at full-scale. The L/D of the actual column is smaller than that studied here to bound the pressures expected.

The permeability of the ion exchange resins was averaged over each step of the loading and regeneration. The results of these tests are shown in Fig. 5. This column permeability, K, was calculated according to Equation.

$$K = \frac{L\mu q}{\Delta p} \tag{4}$$

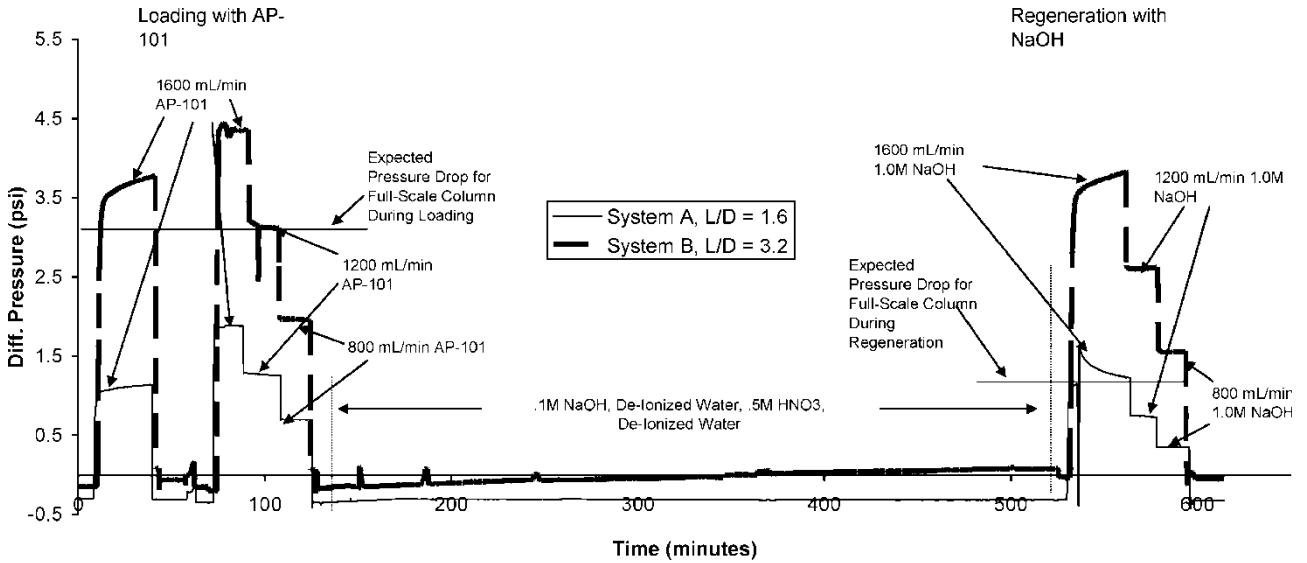

Figure 4. Representative pressure drop profile for a complete load/elute/regenerate cycle as compared to the expected pressure drop for the full-scale column design (SL-644 resin 4th cycle data).

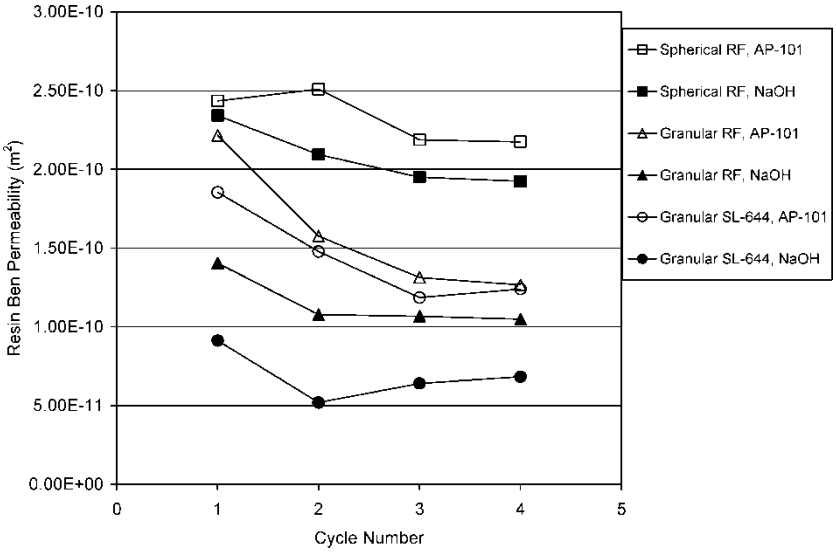

Figure 5. Summary of permeability results from bench scale hydraulic testing for the spherical RF, granular RF, and granular SL-644 resins during loading in AP-101 simulant and during regeneration in NaOH for a height to diameter ratio of 2.8.

where

L = resin bed height, m

q = superficial liquid velocity, m/s

μ = solution viscosity, kg/m/sec

Δp = pressure drop measured across the column, kg/m/sec^2.

The highest permeability was found with the spherical RF resin. Based on the wide range of particle sizes seen in granular resins (described later), it was not surprising that these two resins would have lower bed permeablities than the nearly mono-disperse spherical resin. It is surprising that the SL-644, although it has the largest particle size, had the lowest permeability. As seen in Fig. 5, all resins showed a decrease in permeability from Cycle 1 to Cycle 4.

The maximum liquid differential, radial, and axial pressures measured for each of the resins for the column with an L/D $\sim$2.7 for loading and regeneration are shown in Figs. 6 and 7. In all cases, the load-cell pressures during regeneration were significantly higher than the liquid differential pressure. In general for all resins, the liquid differential pressure was higher processing the simulated supernate than during regeneration. Conversely, the load-cell pressures (both axial and radial) were higher during the regeneration than processing the simulated supernate. The load-cell data also indicated that axial

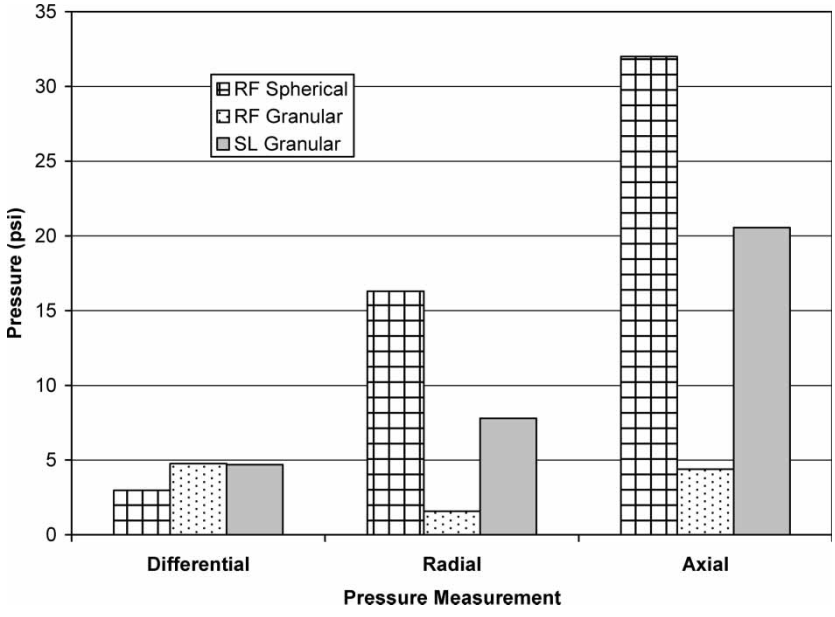

Figure 6. Differential, radial, and axial pressures exerted on the column with a height to diameter ratio of 2.8 during loading with AP-101.

pressures were higher than radial pressures processing the simulated supernate whereas radial pressures were generally higher than axial pressures during regeneration.

The higher liquid-differential pressure processing the simulated supernate was simply the result of a higher viscosity solution. However, the higher load-cell pressures during regeneration indicated that the resins were expanding faster than the resin height was increasing, resulting in outward forces on the bottom and side of the column. The higher radial versus axial forces suggested that a larger fraction of the axial forces were relieved by increasing the bed height.

Unlike the RF granular resin that produced bottom and side load-cell pressures similar to the liquid pressure drop while processing the simulated supernate, the spherical RF resin load cells indicated large increases in axial and radial pressure. This result is believed to be due to the expansion of this resin while processing the simulated supernate. Unlike the other resin tests, in which level remained relatively constant while processing the simulated supernate, introducing simulated supernate to the spherical resin bed caused a sudden decrease in column level followed by a slow rise similar to that seen during regeneration. However, unlike the expansion during the regeneration step that caused higher radial pressures, the simulated supernate expansion for spherical resin resulted primarily in higher axial pressures. The reason for this difference is not clear.

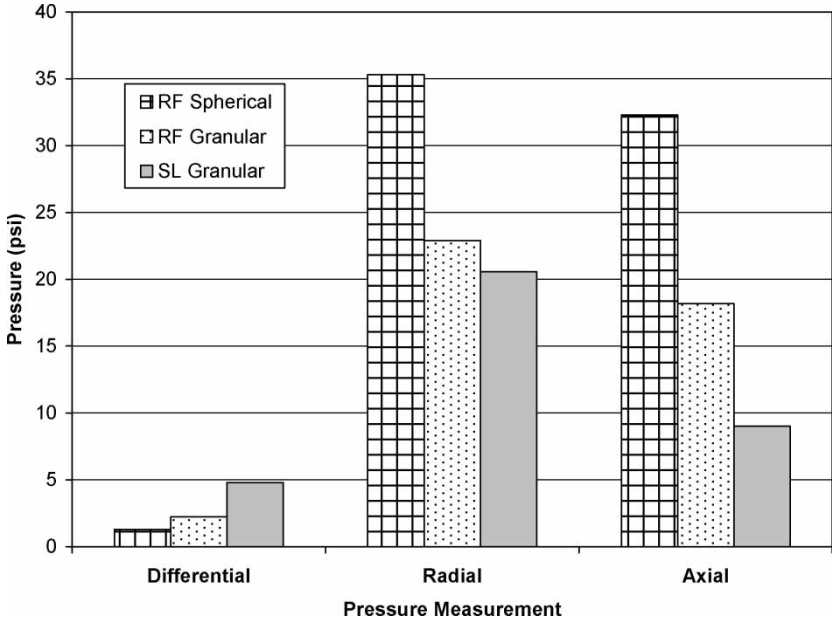

Figure 7. Differential, radial, and axial pressures exerted on the column with a height to diameter ratio of 2.8 during regeneration with NaOH.

In all cases, once flow was stopped, the load-cell pressure dropped quickly to zero (within less than a minute). It appeared that a small liquid differential pressure on the bed held the resin in place and allowed higher load-cell pressures in the bottom of the column. Without the liquid differential pressure, the bed quickly expanded in the vertical direction, relieving all internal pressure. This sudden decrease in load-cell pressure, not seen in previous work performed on the larger scale columns, may occur because of the low coefficient of friction for the glass column sides as compared to the plastic columns used in previous research or may be due to the reduced overall weight of the resin bed due to its smaller size. To prevent this reduction in load-cell pressures, future tests will not allow flow to stop and the columns will be fabricated of a similar stainless steel as seen in the full-scale column.

Particle size measurements were made on representative samples of the resin bed in the hydrogen form both before and after testing. The particle size distribution measurements were performed using a Micro TRAC S3000 Particle Size Analyzer. Results are presented based on volume weighted average. Optical microscopy was also performed to view any particle breakage. In both cases, data indicated a reduction in particle size occurred during testing of the granular RF and SL-644. Figure 8 shows the mean particle size results for the resins before and after testing in the two columns. The granular RF shows a decrease of approximately 80 microns

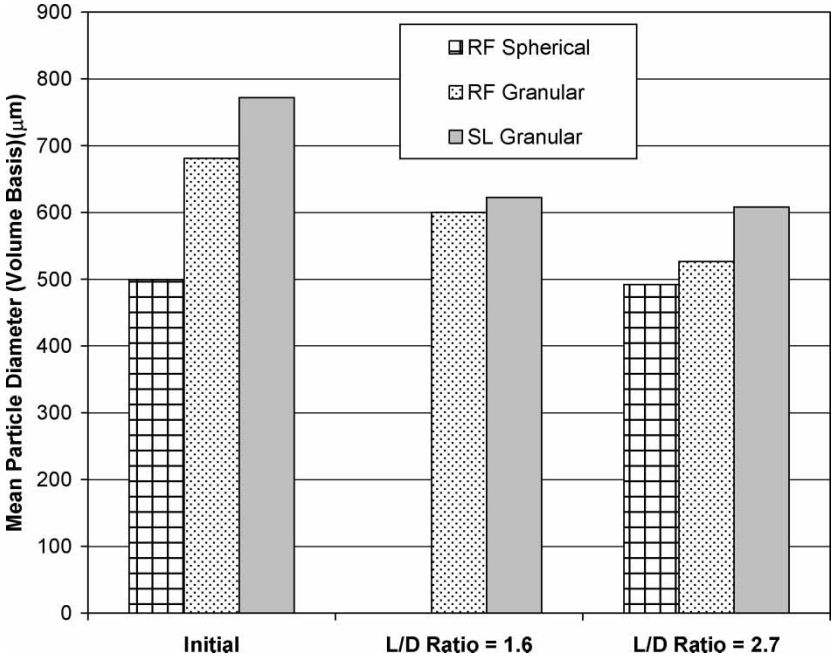

Figure 8. Change in particle size after four cycles in the Bench-Scale Hydraulic Testing System.

and the granular SL shows a decrease of approximately 150 microns in the mean particle size from the beginning to end of the testing. In general, the size distribution for SL-644 was bimodal. Before testing the ~730 micron peak accounted for 60% of the particles and the ~360 micron peak accounted for 14%. After testing, the larger particle fraction decreased to 52% and the smaller particle fraction increased to 35%.

For both granular resins, there was little difference in the particle-size change between the two column tests. Although the column with L/D ratio of 2.7 had greater internal pressures during the testing, the particles did not appear to break up more than the lower L/D ratio column. This may indicate that particle breakage was not necessarily caused by the column forces but the osmotic shock of cycling from acid-to-base form of the resin or from degradation due to chemical or oxygen exposure.

The particle size change of the spherical RF showed very little change in the particle size distribution (PSD) in spite of the large forces exerted on the resin during testing. The micrographs confirmed this result. The number of broken spheres was roughly similar for both the pre-testing and post-testing samples. This is in contrast to the micrographs of the other two resins where many of the particles appear significantly smaller. PSD measurements were not taken on the spherical RF resin for Column A (L/D ratio = 1.6), so no PSD comparison

could be made. However, the micrographs seem to indicate no additional particle breakage from the higher L/D ratio of Column B over Column A.

Five successive compressibility cycles from 0 to 20 psig were performed for each ion exchange resin. The bed was allowed to equilibrate for approximately five minutes between each compressibility cycle. Both the resin height and the force on the side (radial pressure) and the bottom load cells (axial pressure) changed over all five cycles. The resin heights for the final loading cycle are presented in Fig. 9. These results are fairly consistent with previous cycles in that the spherical RF resin showed the least compression ($\sim$0.2 mm or a height ratio of 0.84) and granular SL-644 showed the greatest compression ($\sim$6.3 mm or a height ratio of $>$0.99) over the pressure range studied. This large compressibility is not related to the ground aspect of the material since it was not seen with the ground RF. This high compressibility suggests that the spaces between resin particles could be reduced under higher pressure drops conditions. The reduced bed porosity in turn would increase hydraulic pressure drop and could result in further particle breakage. Thus, high compressibility could result in premature column blockage similar to what was seen in the Savannah River work alluded to earlier.

DISCUSSION

Table 3 provides a summary of the properties of the three resins evaluated in this study. It is interesting to note that the higher expansion pressure of the

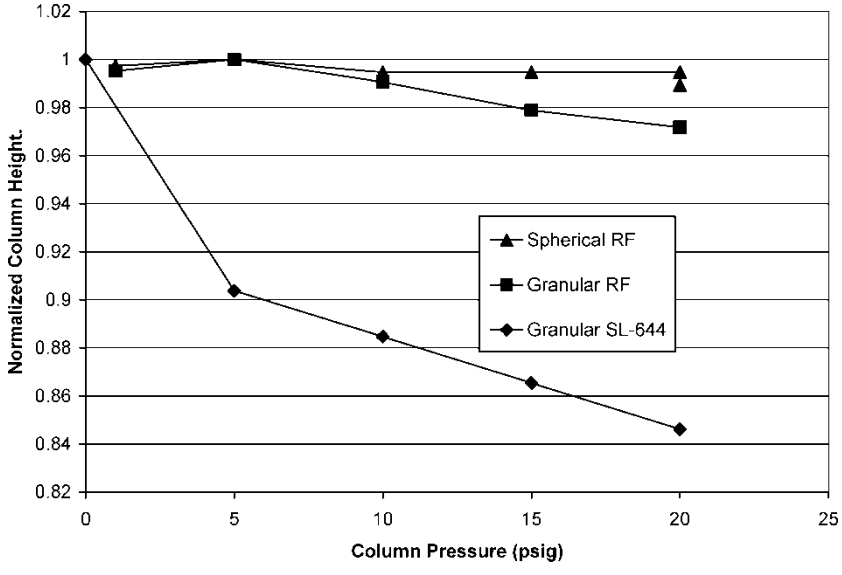

Figure 9. Resin bed height compression as a function of exerted axial pressure.

Table 3. Summary of properties measured during hydraulic testing

Property	Units	Spherical RF	Granular RF	Granular SL
Permeability[a]	m^2	1.92×10^{-10}	1.05×10^{-10}	6.83×10^{-11}
Expansion Pressure[b]	psi	35.3	22.9	20.6
Particle Size Change[c]	μm	7	154	164
Compressibility[d]	dimensionless	0.99	0.97	0.85

[a]Average permeability in cycle #4 for 1600 mL/min of NaOH and the column L/D = 2.7.
[b]Highest pressure exerted in cycle #2 for 1600 mL/min and the column L/D = 2.7.
[c]Change in particle size from pre-testing to post testing based on column L/D = 2.7.
[d]Fractional height decrease at 20 psi for the last cycle.

spherical RF resin did not result in increased particle breakage or in a significant reduction in permeability. It appears that the spherical RF is more durable than the granular materials, thus there is less compressibility and little particle breakage. Rather than fracturing, the resin tends to develop high axial and radial pressures within the column. In contrast, the SL-644 resin does not develop as high pressures; instead it tends to fracture or compress under the load arising from its expansion during regeneration.

The significant compressibility and particle size reduction for the SL-644 could be a concern in a full-scale column. This can be illustrated based on the Blake-Kozeny relationship between pressure drop and void fraction for laminar flow (5):

$$\Delta P = \frac{150\mu(1-\varepsilon)^2 u_o L}{\varepsilon^3 d_p^2} \tag{5}$$

where

L = resin bed height, m

u_o = superficial liquid velocity, m^3/s

ε = bed void fraction

d_p = resin particle size, m

μ = solution viscosity, kg/m/sec

ΔP = pressure drop measured across the column, $kg/m/sec^2$.

By assuming that the column height reduction results in a proportional reduction in bed-void fraction, it is possible to estimate the effect of compressibility on the full-scale column pressure drop. Figure 10 illustrates that

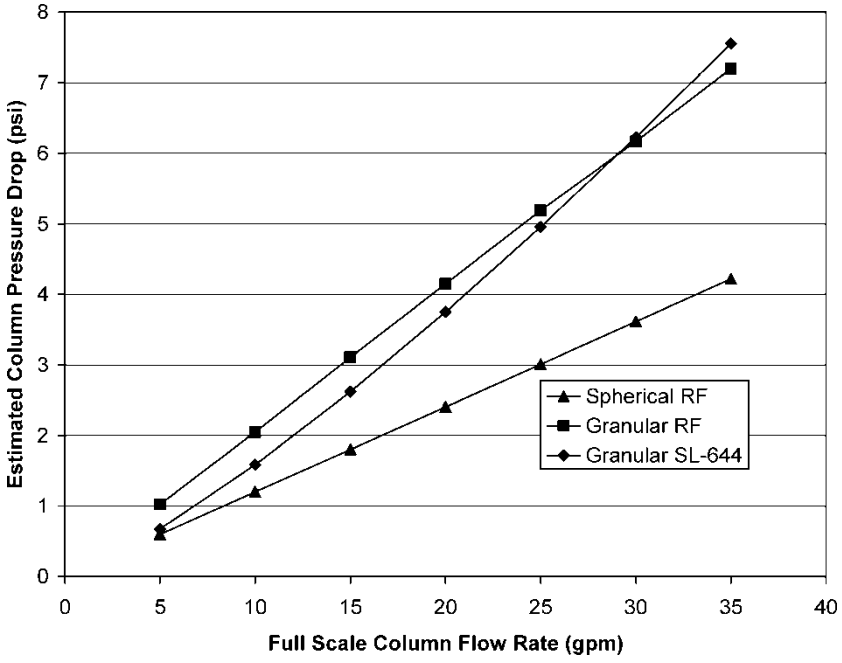

Figure 10. Pressure drop estimated across a full-scale column based on permeability and compressibility data developed for the bench-scale system.

although the column pressure drop for SL-644 is lower than granular RF resin at low flow rates, it rises more quickly with increased flow rates because of the bed compression.

CONCLUSIONS

A method has been developed to compare the hydraulic properties of permeability, particle breakage, column internal pressure, and compressibility for organic ion exchange materials by creating hydraulic conditions within a small scale column similar to those expected in the full-scale unit. While the conditions may not be identical to those seen in the pilot-scale testing done previously, these tests do show trends and provide a means of comparing materials for hydraulic behavior on a small scale. This is accomplished by scaling the superficial velocity within the small-scale column by the ratio of the full-scale to small-scale column height while maintaining the same height to diameter ratio achieves dynamic similarity. The time and costs associated with these hydraulic tests on a small scale are significantly reduced as compared to pilot scale testing.

This approach was performed on granular and spherical RF, and SL-644 resins as part of a study to evaluate RF resins as an alternative to the Hanford

baseline SL-644. The pressure drops at these increased velocities were consistent with those expected in the full scale column. Furthermore, the load cell results were similar to those seen in previous pilot-scale testing.

Radial and axial pressures were monitored during permeability testing as a function of process step and process cycle. The spherical resins produced the highest permeability, while the SL-644 granular resin produced the lowest. The PSD of the spherical resin did not change significantly; however the granular materials (especially SL-644) resulted in a bimodal distribution indicative of significant particle breakage.

By simulating the compressive forces of 20 psig (the highest expected in a full-scale column), the compressibilities of the resins could be estimated. For these tests, the SL-644 compressed volume was significantly greater than the RF resin types. Based on these data, the expected pressure drops within a full-scale column could be predicted. The highest pressures can be expected for a full-scale column of SL-644 because of the significantly higher compressibility of this granular resin.

REFERENCES

1. Peterson, R., Babad, H., Bray, L., Carlson, J., Dunn, F., Pajunen, A., Papp, I., and Watson, J. (2002) *WTP Pretreatment Alternative Resin Selection*; Bechtel National, Inc.: Richland, WA, 24590-PTF-RPT-RT-02-001, Rev. 0.
2. Sundar, P.S. (2002) Pressure drop excursion in ion exchange columns using SuperLig 644 resins for cesium removal. Dec. 4, Memorandum to Todd Wright and Roger Roosa.
3. Fowley, M.D., Steimke, J.L., Adamson, D.J., Hamm, L.L., Nash, C.A., Restivo, M.L., Shadday, M.A., Steeper, T.J., Aleman, S.E., and King, W.D. (2004) *Ion Exchange Testing With Superlig®644 Resin*; Savannah River National Laboratory: Aiken, South Carolina, WSRC-TR-2003-00514, Rev. 0.
4. Russell, R.L., Fiskum, S.K., Poloski, A.P., and Jagoda, L.K. (2002) *AP-101 Diluted Feed (Envelope A) Simulant Development Report*; Pacific Northwest Division: Battelle, Washington, WTP-RPT-057.
5. Bird, R.B., Stewart, W.E., and Lightfoot, E.N. (1960) *Transport Phenomena*; John Wiley & Sons: New York.